



HAL
open science

Characterization and biodistribution of Au nanoparticles loaded in PLGA nanocarriers using an original encapsulation process

Gautier Laurent, Chahrazad Benbalit, Claire Chrétien, Constantin Dupuis, Yann Pellequer, Rana Bazzi, Vivek Sudam Thakare, Franck Denat, Stéphane Roux, Arnaud Béduneau

► To cite this version:

Gautier Laurent, Chahrazad Benbalit, Claire Chrétien, Constantin Dupuis, Yann Pellequer, et al.. Characterization and biodistribution of Au nanoparticles loaded in PLGA nanocarriers using an original encapsulation process. *Colloids and Surfaces B: Biointerfaces*, 2021, 205, pp.111875. 10.1016/j.colsurfb.2021.111875 . hal-03593149

HAL Id: hal-03593149

<https://hal.science/hal-03593149v1>

Submitted on 13 Jun 2023

HAL is a multi-disciplinary open access archive for the deposit and dissemination of scientific research documents, whether they are published or not. The documents may come from teaching and research institutions in France or abroad, or from public or private research centers.

L'archive ouverte pluridisciplinaire **HAL**, est destinée au dépôt et à la diffusion de documents scientifiques de niveau recherche, publiés ou non, émanant des établissements d'enseignement et de recherche français ou étrangers, des laboratoires publics ou privés.



Distributed under a Creative Commons Attribution - NonCommercial 4.0 International License

Characterization and biodistribution of Au nanoparticles loaded in PLGA nanocarriers using an original encapsulation process

Gautier Laurent^{a,b}, Chahrazad Benbalit^{a,b}, Claire Chrétien^a, Constantin Dupuis^a, Yann Pellequer^a, Rana Bazzi^b, Vivek Sudam Thakare^c, Franck Denat^c, Stéphane Roux^{b,*} and Arnaud Béduneau^{a,*}

^a PEPITE EA4267, Université de Bourgogne Franche-Comté, F-25030 Besançon, France.

^b Institut UTINAM, Université Bourgogne Franche-Comté, UMR 6213 CNRS-UBFC, 25030 Besançon Cedex, France

^c Institut de Chimie Moléculaire de l'Université de Bourgogne (ICMUB), Université Bourgogne Franche-Comté, UMR 6302 CNRS-UBFC, 21078 Dijon Cedex, France

* : Corresponding authors:

E-mail : arnaud.beduneau@univ-fcomte.fr

E-mail: stephane.roux@univ-fcomte.fr

Abstract

Due to their imaging and radiosensitizing properties, ultrasmall gadolinium chelate-coated gold nanoparticles (AuNP) represent a promising approach in the diagnosis and the treatment of tumors. However, their poor pharmacokinetic profile, especially their rapid renal clearance prevents from an efficient exploitation of their potential for medical applications. The present study focuses on a strategy which resides in the encapsulation of AuNP in large polymeric NP to avoid the glomerular filtration and then to prolong the vascular residence time. An original encapsulation procedure using the polyethyleneimine (PEI) was set up to electrostatically entrap AuNP in biodegradable poly(lactic-co-glycolic acid) (PLGA) and polyethylene glycol -PLGA (PLGA-PEG) NP. Hydrodynamic diameters of NP were dependent of the PEI/Au ratio and comprised between 115 and 196 nm for ratios equal or superior to 4. Encapsulation yield was close to 90% whereas no loading was observed without PEI. No toxicity was observed after 24hr exposure in hepatocyte cell-lines. Entrapement of AuNP in polymeric

nanocarriers facilitated the passive uptake in cancer cells after only 2hr incubation. In healthy rat, the encapsulation allowed increasing the gold concentration in the blood within the first hour after intravenous administration. Polymeric nanoparticles were sequestered in the liver and the spleen rather than the kidneys. T₁-weighted magnetic resonance demonstrated that encapsulation process did not alter the contrast agent properties of gadolinium. The encapsulation of the gold nanoparticles in PLGA particles paves the way to innovative imaging-guided anticancer therapies in personalized medicine.

Statistical summary of the article

5 727 words; 1 table; 7 figures

Keywords

Gold nanoparticles, PLGA nanoparticles, MRI, gadolinium, theranostic

1. Introduction

Due to their optical and radiosensitizing properties, the use of gold nanoparticles (AuNP) in biomedical applications represents a promising strategy, especially in the treatment of cancer¹⁻⁴. By absorbing near infrared photons, they can trigger a local heating, leading to a cytotoxic effect. Moreover, the high atomic number of the Au atom allows a high absorption of ionizing radiations such as X and γ radiations, increasing the damages caused to target cells during the radiotherapy⁵⁻⁷.

Recently, Roux *et al.* developed a theranostic approach using multifunctional AuNP. The aim was to enhance radiotherapy effects in the tumoral zone and determine the best moment for irradiation by monitoring the accumulation in the tumor by Magnetic Resonance Imaging (MRI). For achieving MRI-guided radiotherapy AuNP were coated with different polyaminocarboxylate chelators (DTDTPA, TADOTAGA) which form stable complexes with gadolinium (III) ions (Gd³⁺), a contrast agent

frequently used in MRI. The immobilization of gadolinium ions on the surface of TADOTAGA-coated AuNP confers to the latter a behavior of positive contrast agent for MRI. The TADOTAGA chelator was mainly composed of a macrocyclic polyaminocarboxylate and of sulfur atoms to allow the anchorage on the AuNP². Gd³⁺ complexes of such DOTA-derivatives are known to be more stable and biologically inert, compared with linear DTPA-derived chelators. In addition, they were able to chelate other atoms such as ¹¹¹In and ⁶⁴Cu for SPECT and PET imaging, respectively. The treatment of rats bearing a 9L gliosarcoma by radiotherapy 10 minutes after intravenous injection of AuNP significantly enhanced their lifespan. The increase of the survival time is assigned to the radiosensitizing effect of the gold core. However, the AuNP were characterized by a short half-life in blood due to a rapid renal clearance. Moreover, the small size of NP limits the passive targeting of solid tumors mediated by the enhanced and permeability effect (EPR effect)⁸. An increase of the hydrodynamic diameters of AuNP could overcome these limitations but would alter dramatically the radiosensitizing properties of nanoparticles and their elimination from the organism by renal clearance⁹⁻¹¹.

In the present study, a strategy residing in the encapsulation of small AuNP in large biodegradable polymeric NP was investigated to improve their pharmacokinetic profile and their biodistribution by preserving their radiosensitizing properties. Only after accumulation in tissues and polymer biodegradation, AuNP will be released from NP, allowing their renal elimination. Poly(lactic-co-glycolic acid) (PLGA) conjugated or not with polyethylene glycol (PEG) was used as biodegradable polymer. PEG is known to prolong the vascular residence time of NP by limiting the opsonization process and consequently the recognition of particles by the Kupffer cells^{12,13}. The original encapsulation procedure of AuNP in polymeric particles was based on the addition of a cationic polyelectrolyte, the polyethyleneimine (PEI), during the solvent displacement process. The effects of PEI/Au ratio on the physicochemical properties of nanoparticles were investigated. In vitro studies using hepatic and cancer cells were performed to study the cytotoxicity and the cell internalization of AuNP entrapped in PLGA particles. Pharmacokinetic and biodistribution studies of polymeric NP were finally carried out in healthy rats to characterize the long-circulating properties and the elimination pathway of AuNP.

2. Materials and methods

2.1. Materials

The following chemicals were obtained from commercial suppliers and used as received: The polymer poly (D,L-lactic- co- glycolic acid) 50:50 (PLGA ; MW 7,000-17,000) was purchased from Evonik Industries (Evonik Röhm GmbH) and poly (D,L-lactic- co- glycolic acid) -polyethyleneglycol 50:50 (PLGA :MW 25000 Da, PEG : MW 5000 Da) under the commercial name of Resomer® RG 502H was purchased from Sigma Aldrich (St-Quentin Fallavier, France). Chloroauric acid ($\text{HAuCl}_4 \cdot 3\text{H}_2\text{O}$), sodium borohydride (NaBH_4), PVA (polyvinyl alcohol) MW 30000-70000, branched polyethylenimine (PEI) MW 25000, gadolinium chloride ($\text{GdCl}_3 \cdot 6\text{H}_2\text{O}$), dimethylsulfoxide (DMSO) were purchased from Sigma Aldrich (St. Louis, MO, USA). TA-DOTAGA ligand was obtained from CheMatech® (Dijon, France).

2.2. Synthesis of AuNP

The synthesis was adapted from the single-phase protocol developed by Brust *et al*¹⁴. AuNP were obtained by reduction of the gold salt ($\text{HAuCl}_4 \cdot 3\text{H}_2\text{O}$) using NaBH_4 in presence of TADOTAGA ligand. Adsorption of TADOTAGA on the NP surface controls the size and the colloidal stability and allows the immobilization of gadolinium. For a typical preparation of AuNP, $\text{HAuCl}_4 \cdot 3\text{H}_2\text{O}$ (50 mg, 1.22×10^{-4} mol), dissolved in methanol (20 mL), were placed in a 250 mL round-bottom flask. An aqueous solution of TADOTAGA chelator (86 mg, 1.22×10^{-4} mol in water (10 mL)) was added to the gold salt solution under stirring. The mixture turned from yellow to orange. After a few minutes, NaBH_4 (48 mg, 12.7×10^{-4} mol) dissolved in water (3 mL) was added to the mixture under vigorous stirring at room temperature. The stirring was maintained for 1 h. Then, the mixture was dialyzed using a 6,000-8,000 kDa MWCO membrane.

To obtain final suspension of AuNP ($[\text{Au}] = 51 \text{ mM}$, $[\text{Gd}] = 5 \text{ mM}$) before encapsulation process, gold suspension was concentrated, and gadolinium was entrapped within the TADOTAGA chelator by stirring overnight the suspension with $\text{GdCl}_3 \cdot 6\text{H}_2\text{O}$ (370 μL at 135 mM for a typical 10 mL AuNP

suspension). The gadolinium concentration of 5 mM guarantees the suspension stability and an optimal MRI signal.

2.3. Synthesis of AuNP -loaded PLGA NP

The synthesis of polymeric NP was based on a nanoprecipitation process by solvent displacement¹⁵. For a typical preparation of NP3 (Table 1) corresponding to a PEI/Au ratio equal to 5, a suspension of AuNP (25 μ L, 10mg/mL (*i.e.* 51 mM)) was mixed with an aqueous solution of PEI (25 μ L, 5% w/w). HCl 1N was previously added in the PEI solution to reach a hydrodynamic diameter of NP3 close to 160 nm \pm 15 nm. PEI/Au ratio modulation was performed by adjusting the PEI concentration of the stock solution to add equal volumes of AuNP suspension at 10mg/ml and PEI solution (25 μ l). The same HCl volume than for the NP3 preparation was added to the solution, independently of the PEI concentration. The AuNP suspension containing PEI was added in 1ml of PLGA or PLGA-PEG solutions in DMSO at 15mg/mL and 18mg/mL, respectively. Then 4 mL of PVA dissolved in water at 0.75% was added gradually to the mixture, previously vortexed.

For the preparation of NP3 by adsorption of AuNP (adsorbed), PLGA NP were previously formed following the same protocol than conventional NP3. Then, 5% PEI solution (25 μ L) was transferred in the suspension of PLGA nanoparticles under stirring. After 5 minutes of incubation, a suspension of AuNP (25 μ L, 10mg/mL (*i.e.* 51 mM)) was finally added to the PEI-coated PLGA nanoparticles.

The various preparations were washed three times by ultracentrifugation at 30,000g for 1 h, at 4°C to remove free AuNP. Finally, they were freeze-dried using sucrose as cryoprotector except in batches used for estimating the production yield, the encapsulation yield and rate. These following parameters were calculated as follows:

$$\text{Production Yield (\%)} = \frac{\text{Amount of freeze-dried PLGA NP}}{\text{Amount total of polymer for the preparation of NP}} \times 100 \quad (1)$$

$$\text{Encapsulation Yield (\%)} = \frac{\text{Amount of gold in freeze-dried PLGA NP}}{\text{Amount total of Au for the preparation of NP}} \times 100 \quad (2)$$

$$\text{Encapsulation Rate (\%)} = \frac{\text{Amount of gold in freeze-dried PLGA NP}}{\text{Amount of freeze-dried PLGA NP}} \times 100 \quad (3)$$

2.4. Size and Zeta Potential Measurements

The hydrodynamic diameter and the Zeta potential of NP were measured using a Zetasizer Nano ZS90 (Malvern Instruments, UK). Samples were diluted ten times prior to the measurements. Size and the polydispersity index (PDI) were determined by dynamic light scattering at 25°C. The Zeta potential determination was performed by laser Doppler electrophoresis at 25°C. NaCl was added in the diluted NP suspension to reach a concentration of 0.01 M.

2.5. Transmission electron microscopy (TEM) and scanning transmission electron microscopy (STEM).

TEM and STEM were respectively used to obtain detailed morphological information and AuNP localization for every sample. Characterizations were performed on a JEOL 2100F microscope operating at 200 kV. NP3 (PEI/Au ratio =5) were previously stained with 1% phosphotungstic acid and whased by ultracentrifugation. The samples were prepared by depositing a drop of a diluted colloidal solution onto a carbon membrane supported by copper grid and left in air at room temperature until complete drying was achieved.

2.6. MRI Phantoms

Eppendorf tubes containing NP suspension including Au NP, NP3 and NP3-PEG characterized by a PEI/Au ratio of 5 were imaged at 7T at different concentrations using an inversion–recovery FLASH(IR-FLASH) imaging sequence with varying IR. T_1 -weighted contrast enhancement was controlled running a standard Spin–Echo (SE) sequence with 500 ms TR and 12 ms TE. Datas were treated with image J.

2.7. Cell lines and cell culture

9L Rat malignant glioma cells and HepG2 were purchased from American Type Culture Collection (ATCC). 9L were cultivated in Dulbecco's Modified Eagle's Medium (DMEM) with GlutaMax, 10% FBS and 1% antibiotic (100µg/ml streptomycin and 100U/ml penicillin). HepG2 cell lines were cultivated in Dulbecco's Modified Eagle's Medium (DMEM) with GlutaMax, 10% FBS, 1% non-

essential amino acids and 1% antibiotic (100µg/ml streptomycin and 100U/ml penicillin). Cells were cultivated at 37°C with 5% CO₂, under humidified atmosphere.

2.8. MTS viability assay

HepG2 and 9L cell-lines were seeded in 96-well plates at a density of 100,000 cells per well. NP3 previously freeze-dried with sucrose as cryoprotective agent at a PLGA: sucrose ratio of 1:0.8 were resuspended in HBSS culture medium. NP3 suspensions (PEI/Au ratio = 5) were incubated with HepG2 during 24 hrs and 2hrs for 9L. PLGA concentrations ranged from 10mg/ml to 0.5mg/ml corresponding to a gold concentration comprised between 140 and 7µg/ml. AuNP were diluted in HBSS to reach the same gold concentrations as for NP3 suspensions. Controls were performed with HBSS and a sucrose solution at 8mg/ml corresponding to the highest PLGA concentration (10 mg/ml). After incubation, cells were washed 3 times with HBSS. A colorimetric cell viability assay was then performed after addition of 100µl of HBSS and 20µl of a mixture of 3-(4,5-Dimethylthiazol-2-yl)-5-(3-carboxymethoxyphenyl)-2-(4-sulfophenyl)-2H-tetrazolium (MTS, Promega) and phenazine methosulfate (PMS, Promega). Incubation was performed during at least 1hr at 37°C with 5% CO₂, under humidified atmosphere. The absorbance was then measured at 490 nm with a microplate reader (Synergy HT BioTek).

2.9. Internalization experiment

9L cellular uptake of NP3 (PEI/Au ratio = 5) and AuNP was evaluated at 4°C and 37°C with or without 30min-pretreatment with 20 mM sodium azide, an endocytosis inhibitor. 9L cells were seeded in 6 wells plates at a density of 300,000 cells/well. Freeze-dried nanoparticles were resuspended in HBSS at a final PLGA concentration of 1mg/ml and transferred in wells. AuNP suspensions were prepared in HBSS at a concentration in the same range as gold concentrations in the NP3 (14µg/ml) suspension. Nanoparticles were incubated with 9L for 2 hours. After incubation, media was removed, and the cells were gently washed 3 times with HBSS. NaOH at 0.1N was then added in each well. After homogenization, supernatant was split in two equal volumes for the separate estimations of gold and protein amounts. Protein concentrations were determined using a BCA protein assay (ThermoScientific) with a bovine

serum albumin standard curve. Gold content in cells was assessed by ICP-OES (Varian) and the quantity was normalized with the protein amount determined by BCA.

2.10. Animals

All experimental procedures were approved by the local committee for ethics in animal experimentation (n° 2012/001-CD) of Franche-Comté University (Besançon, France), and complied with the Guide for the Care and Use of Laboratory Animal published by the US National Institutes of Health (NIH publication No. 85–23, revised 2011). Six-week-old male Sprague Dawleys rats were purchased from Janvier (Le Genest Saint Isle, France). The animals were maintained under a 12-hours light/dark cycle and a temperature and hydrometry-controlled environment. Food and water were provided *ad libitum*. A total of 32 rats were used for the animal experiment and were divided in 9 groups. 3 groups were used for each preparation (AuNP, NP3 and NP3-PEG) including 2 groups (n=3) for the pharmacokinetic and the biodistribution studies at 0.5h and 2h and 1 group (n=5 except for the NP3-PEG where n=4) for the time point 24h.

2.11. Biodistribution and pharmacokinetic experiments

Freeze-dried NP were reconstituted under class II biological safety cabinet in 10 mM sterile HEPES buffer to reach a PLGA concentration of 100 mg/mL. Osmolarity was close to 300 mOsmol/l due to the presence of sucrose used as cryoprotective agent for the freeze-drying. NP suspension (0.5 mL) including Au NP, NP3 and NP3-PEG characterized by a PEI/Au ratio of 5 were immediately injected in rat under isoflurane anesthesia by the penile vein. At 0.5h, 2h and 24h following the NP injections, rats were anesthetized with sodium pentobarbital (50 mg/kg; intraperitoneal) and blood samples were collected by the tail vein. Sacrifice of animals were performed under pentobarbital anesthesthesia followed by a cardiac perfusion with saline for 10 minutes. The liver, the kidneys, the spleen, the lungs, the intestine, the heart and the penis were then collected and stored at -80°C. Blood samples were also collected at 1h in the groups of rats sacrificed at 2h.

2.12. Gold titration in biodistribution studies

Samples were weighed and digested by heating at 90°C in 5 mL of aqua regia mixture (1:3 HNO₃/HCl), then they were diluted to 50 mL with HNO₃ (2%) solution. A calibration curve was prepared by successive dilutions of a gold solution in 2% HNO₃. Organ samples (liver, spleen, intestine, lungs, kidneys, heart and penis) were analyzed by atomic absorption spectroscopy AAS 240 FS (Agilent) and blood samples by ICP-OES (Varian). The Au content in each organ was expressed as the percentage of injected Au dose per g of tissue.

2.13. MRI

The rat was anesthetized under pentobarbital, then the NP3 suspension (PEI/Au ratio =5) was injected by the penile vein. The injected volume was set to 0.5 mL and the PLGA concentration was fixed at 100 mg/mL. Images were acquired before and at 5 and 20 minutes following the injection using a 1.5T MRI system (General Electric Healthcare, Signa Explorer). *T*₁-weighted images were obtained in the coronal plane using the following sequence parameters: TE = 8.9 ms, TR = 403 ms, Thickness = 2.2 mm, Sp= 0.5mm.

3. Results and discussion

3.1. Influence of PEI/Au ratio on the encapsulation of AuNP-loaded PLGA NP

Table : 1 Characteristics of AuNP-loaded PLGA NP. Values were reported as mean \pm standard deviation (n=3).

Formulation	AuNP	NP1	NP2	NP3	NP4	NP5	NP6	NP3- PEG	NP3' (PEI adsorbed)
PEI/Au ratio		8	6	5	4	0 <...< 4	0	5	5
AuNP (mg)		0.25	0.25	0.25	0.25	0.25	0.25	0.25	0.25
Hydrodynamic Diameter (nm)	7 \pm 2	115 \pm 6	135 \pm 19	159 \pm 14	196 \pm 11		136 \pm 4	198 \pm 5	153 \pm 3
Polydispersity Index		0.15 \pm 0.03	0.16 \pm 0.03	0.16 \pm 0.01	0.17 \pm 0.03	Aggregates	0.05 \pm 0.02	0.17 \pm 0.03	0.07 \pm 0.00
Zeta Potential (mV)	-20.5 \pm 2.1	5.8 \pm 1.2	4.8 \pm 0.6	3.2 \pm 0.7	1.2 \pm 0.7		-0.8 \pm 0.2	3.7 \pm 0.6	0.6 \pm 0.1
Production Yield (%)		38 \pm 10	54 \pm 9	71 \pm 7	82 \pm 6		35 \pm 5	54 \pm 5	64 \pm 3
Encapsulation Yield (%)		94 \pm 7	102 \pm 5	95 \pm 8	88 \pm 7		2 \pm 2	86 \pm 6	52 \pm 7
Encapsulation Rate (%)		1.4 \pm 0.1	1.5 \pm 0.1	1.4 \pm 0.2	1.3 \pm 0.1		0.0 \pm 0.0	1.1 \pm 0.0	0.7 \pm 0.1

Prior to the encapsulation, AuNP were co-incubated with PLGA and PEI at different PEI/Au ratio. NP were then produced by solvent displacement method using DMSO. Hydrodynamic diameters of PLGA NP increased from 115 nm \pm 6 nm to 196 nm \pm 11 nm when ratio decreased from 8 to 4. For the four first preparations, the polydispersity index (PDI) was inferior to 0.2, demonstrating a homogeneous size distribution. Besides, the Zeta potential of particles was dependent on the PEI content. This result demonstrates the adsorption of a part of PEI on the NP surface despite the presence of non-ionic surfactant PVA. For ratio strictly inferior to 4, an aggregation of PLGA NP was observed whereas the lack of polycation led to the formation of 136 nm NP with a narrow size distribution (NP6). The addition of polycation allowed encapsulating approximately 90 % of AuNP in PLGA whereas the

encapsulation yield was close to 0 without it, demonstrating the key role of PEI in the entrapment process. This could be explained by the electrostatic interactions of negatively charged carboxylate groups located both in the organic shell of AuNP nanoparticles and in the PLGA (resomer RG502H) with the positively charged ammonium groups of PEI. A lower encapsulation yield, close to 52%, was observed when PEI was adsorbed on preformed PLGA particles (NP3'). This demonstrates the interest to add the polycation during the nanoprecipitation process for a better entrapment efficiency. The PEI/Au ratio increase from 4 to 8 did not significantly impact the encapsulation yield, unlike the hydrodynamic diameters of NPs which decreased from 196 nm to 115 nm. This result was consistent with the findings of Katas et al. that showed a size reduction of NP from 661 nm and 253 nm when PLGA/PEI ratio dropped from 59:1 to 5:1¹⁶. Another study showed that the association of a negatively charged polyesters with a cationic drug model reduced the size of NPs obtained by a solvent displacement process. This was explained by the "Ouzo region" shift due to the increased aqueous solubility of polymer after complexation with cationic molecules¹⁷. Similarly, electrostatic interactions between PEI and carboxylic end groups of Resomer 502H PLGA could increase the polymer solubility in water, leading to the formation of smaller NPs. By contrast, a low PEI/Au ratio may induce a high density of AuNP complexed to PEI, altering the water-solubility properties of polycation and consequently of the complex PEI/PLGA. This effect could explain the aggregation of NP prepared with PEI/Au ratio inferior to 4.

The production yield of PLGA NP was lower with the highest ratio PEI/Au ratio due to smallest particles that were not collected in the centrifugation steps. An increase of the centrifugation speed would induce a settling out of single AuNP. NP3-PEG were produced with the same PEI/Au ratio as NP3 but PLGA was replaced by PEG-conjugated PLGA (PLGA-PEG). The hydrodynamic diameter was higher owing to the presence of a PEG corona likely in "brush-like" conformation on the particle surface. In addition, due to the lack of carboxylic end groups on the polyester, PEI cannot interact with the PLGA-PEG block polymer in contrast to PLGA. Thus, the role of PEI could be only attributed to the formation of AuNP clusters by electrostatic interactions, facilitating their entrapment in the PLGA-PEG matrix during the nanoprecipitation process. Whereas both the encapsulation yield and rate were

in the same range than the PLGA NP, the production yield of NP3-PEG was lower, close to 50% vs $71\% \pm 7\%$ for NP3. Monomers of PLGA-PEG in the aqueous phase or PLGA-PEG/PVA mixed micelles could be present with PLGA-PEG NP and then removed during the washing steps.

The encapsulation of preformed AuNP in PLGA NP was already tested by other groups. Encapsulation using a water-in-oil-in-water (w/o/w) double emulsion and an oil-in-water (o/w) single emulsion was performed by Luque-Michel *et al*¹⁸. A low encapsulation efficiency was observed with the double emulsion method. To enhance the loading of AuNP in PLGA NP, inorganic particles were concentrated in the inner water phase. However, due to the high concentration, an aggregation of AuNP was observed, leading to a heterogenous size distribution. Another approach using the single emulsion method was performed after functionalization of AuNP with lipophilic ligands to stabilize the particles in ethyl acetate. However, the encapsulation yield was not improved compared with the double emulsion method. In addition, AuNP with the lipophilic coating were not stable, inducing a large size distribution and the presence of empty particles. A work performed by Wang *et al.* focused on the stabilization of silica-coated AuNP and a perfluorohexane liquid using a PLGA shell¹⁹. The particles prepared using a w/O/W double emulsion technique exhibited a size comprised between 0.486 and 9.25 μm , requiring a filtration step prior to the intravenous injection. Thus, the PEI-mediated encapsulation method seems to be a promising and innovative approach to entrap preformed negatively charged AuNP in PLGA NP with a high encapsulation efficiency and an adjustable size in the nanometer range (Table 1). Other alternatives were described in literature consisting mainly in the *in situ* formation of AuNP in PLGA NP¹⁷. However, this strategy does not allow the surface functionalization of AuNP and requires a double emulsion method which is a multiple step complex procedure.

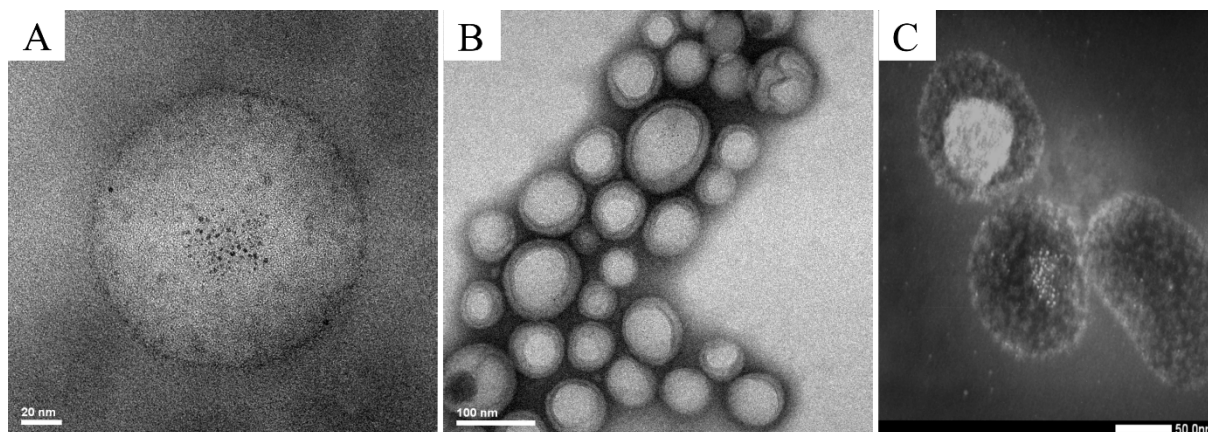


Figure 1: (A, B) Transmission electron micrographs and (C) Scanning transmission electron micrographs of NP3.

Location of AuNP entrapped in PLGA matrix (NP3 : PEI/Au=5) was investigated by electron microscopy in figure 1. NP were heterogeneously distributed in the PLGA matrix, supporting the hypothesis of AuNP clusters formed by electrostatic attractions with PEI.

3.2. Influence of the encapsulation on the contrast agent properties of AuNP

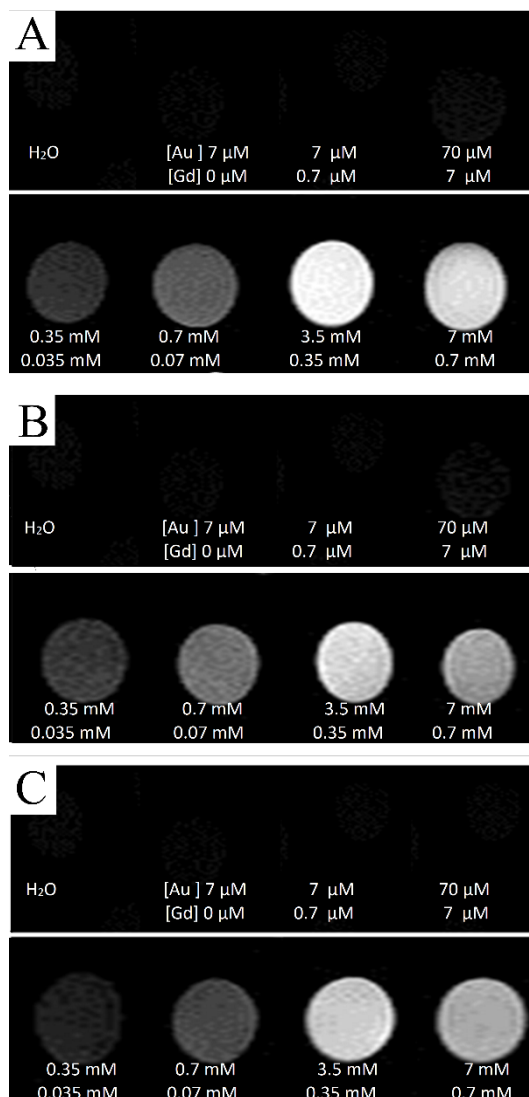


Figure 2: MRI phantom images of AuNP (A), NP3 (B) and NP3-PEG (C). The highest dosages in gadolinium and gold correspond to the concentration of reconstituted suspensions prior to injection.

Effects of the encapsulation process on contrast agent properties of gadolinium chelate-coated AuNP were investigated by acquiring MR images of nanoparticles suspension with different dilution rates. The suspensions of AuNP, NP3 and NP3-PEG (PEI/Au=5) were diluted in deionized water to obtain different Gd concentrations ranging from 0.7 μM to 0.7 mM. The highest gold concentration, *i.e.* 7 mM, corresponded to the injected gold dose for biodistribution and pharmacokinetic studies. Signal intensity of various preparations were observed on the T_1 -weighted MR images in figure 2. A concentration-dependent increase of the signal was observed until 0.35 mM for the different preparations. However, a

signal loss assigned to a predominant T_2^* effect and a T_1 -saturation was observed at 0.7 mM²⁰. Moreover, the evolution of the positive contrast enhancement as a function of Gd^{3+} concentration was very similar between free and entrapped AuNP, suggesting that encapsulation did not affect the imaging properties of gadolinium.

3.3. Comparative study of cell viability and internalization

The physicochemical characterization of NP3 particles (PEI/Au=5) demonstrated that the use of PEI facilitates the encapsulation of the radiosensitizing and paramagnetic AuNP. The next step of the evaluation of these particles lies in the comparative *in vitro* study between free and encapsulated AuNP. First, the cytotoxicity of polymeric nanoparticles was carried out with two different cell-lines including human hepatocellular liver carcinoma cell line (HepG2) and rat brain gliosarcoma cell line (9L). HepG2 cell-lines were used to predict the acute hepatic toxicity of nanoparticles considering that the liver is mainly involved in the elimination of large nanoparticles. 9L tumor cells were chosen as a target cell of AuNP in anticancer therapies. Cytotoxicity study with 9L was performed during 2hrs to select the safe NP concentrations for internalization experiments. Concentrations in PLGA were comprised between 0.01 mg/mL and 10 mg/mL corresponding to gold contents ranging from 0.140 μ g/ml to 140 μ g/ml. They were incubated with 9L and HepG2 for 2hr and 24hrs, respectively. Viability was evaluated by MTS assay (Fig 3). Sucrose control was included in the study due to the presence of this cryoprotective agent in the freeze-dried NP3 preparations. For every gold concentration, the viability of HepG2 and 9L remained above 80%, in the same range as the culture medium and sucrose controls. Thus, AuNP and NP3 were not cytotoxic with both HepG2 and 9L cell-lines up to 10 mg/ml of PLGA and 140 μ g/ml of gold.

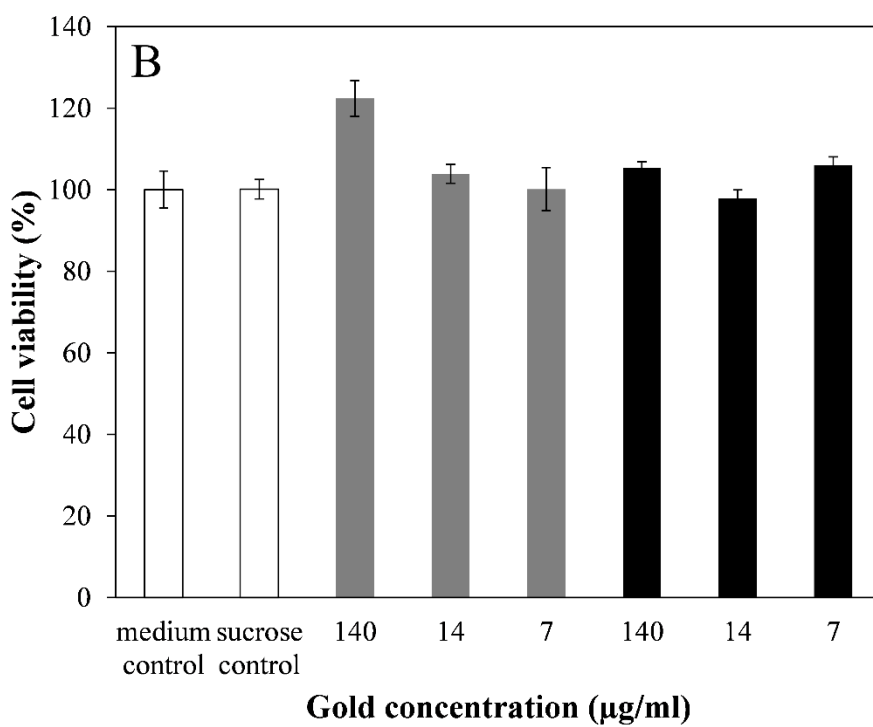
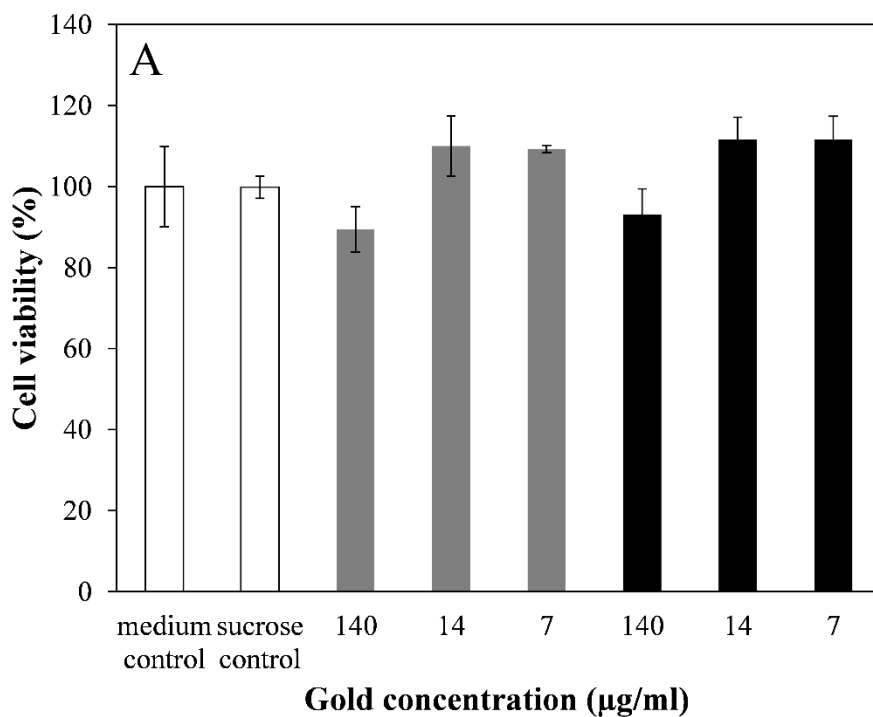


Figure 3: Cell viability evaluated by MTS after incubation with NP3 (gray bars) and AuNP (black bars) for 24h with HepG2 (A) and 2h with 9L cells (B). Gold concentrations were comprised between 140 µg/ml and 7 µg/ml. Values were reported as mean \pm standard deviation (n=4).

A comparative internalization study of NP3 (PEI/Au=5) and free AuNP in 9L cells was performed in three different conditions (2h at 37°C with or without sodium azide and 4°C) to investigate the uptake process. Sodium azide (NaN₃) was used to deplete cells energy by inhibiting the production of ATP. The low temperature (4°C) condition prevents from both, active and passive uptake by inhibiting endocytosis and increasing the plasma membrane rigidity²¹. The internalization of the nanoparticles was monitored by determining the gold amount in cells normalized by the protein content (Figure 4).

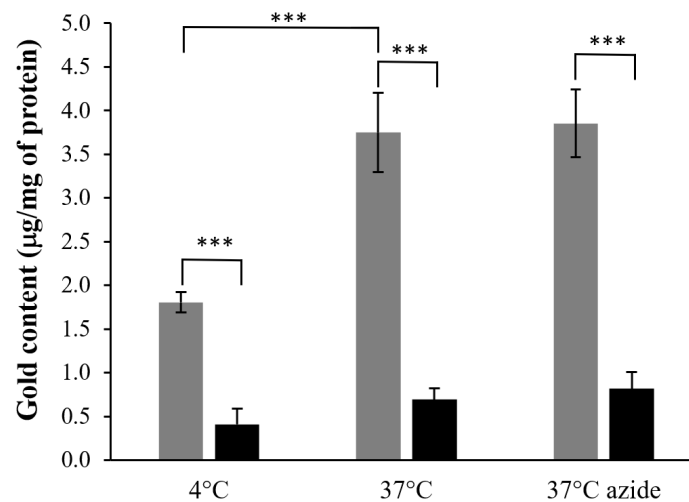


Figure 4: Gold content in 9L cells after 2h-incubation with with NP3 (gray bars) and AuNP (black bars), at 4°C and 37°C with or without sodium azide treatment. Values were reported as mean ± standard deviation (n=6). Statistical analysis was performed using ANOVA followed by a Student-Newman-Keuls test. Results were considered as statistically significant at P<0.001 (***).

A temperature effect on the gold content in 9L cells was noticed for both NP. Highest values were obtained at 37°C. At 4°C, gold amounts were of 0.41 and 1.80 µg/mg protein after incubation of AuNP and NP3 (PEI/Au=5), respectively. At that temperature, only an adsorption process on the cell surface can be hypothesized. It could be facilitated by electrostatic interactions between the negatively charged cell membranes and the positive Zeta Potential of NP3. Considering that sodium azide did not significantly alter the uptake values, the gold content differences observed at 37°C and 4°C suggest the internalization of AuNP and NP3 in 9L cells using a passive process. In addition, the encapsulation of AuNP nanoparticles in PLGA particles facilitated the cell internalization. Values were respectively of

0.69 and 3.75 at 37°C for AuNP and NP3. The surface properties of PLGA nanoparticles, especially the positive charge and the size could influence the uptake process. Chithrani *et al.* demonstrated that the accumulation of ultrasmall nanoparticles is limited in comparison to larger nanoparticles^{22,23}. The internalization study reveals therefore another advantage of the encapsulation of AuNP nanoparticles. A better interaction with cells should optimize the radiosensitizing effect of AuNP. However, the accumulation of the encapsulated radiosensitizing AuNP nanoparticles in cancerous cells after intravenous injection requires also long-circulating properties.

3.4. Pharmacokinetics and biodistribution studies

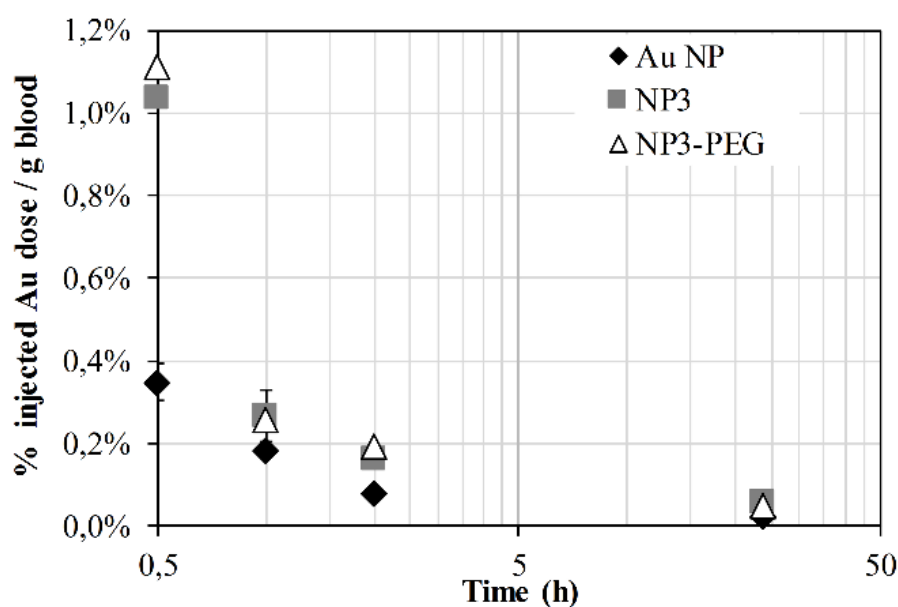


Figure 5: Pharmacokinetics of AuNP, NP3 and NP3-PEG after a single intravenous injection in healthy rat. Blood was collected at 0.5h, 1h, 2h and 24h following the administration. Values were reported as mean \pm standard deviation (n=3).

Free AuNP, NP3 and NP3-PEG (PEI/Au=5) were injected intravenously in healthy rat. Pharmacokinetic profiles of various preparations were shown in figure 5. The gold concentration in blood was determined at different time points by ICP analysis of the collected blood. About 1% of the injected dose (ID) of NP3 and NP3-PEG were still detected in the blood at 0.5h post-injection whereas the value was only of 0.35% for AuNP. At 1h and 2h following the intravenous injection, the gold concentrations were still

higher with polymeric NP compared with free AuNP. At 24h post-injection, the gold concentration in the bloodstream was negligible for the three preparations. The pharmacokinetic profiles of NP3 and NP3-PEG were very close. This similarity can be explained by the presence of PVA adsorbed on the PLGA NP. This hydrophilic non-ionic polymer used as stabilizer in the preparation of polymeric NP could confer a hydrophilic steric barrier against opsonization in the same way as the PEG corona. In accordance with this hypothesis, Takeuchi *et al.* showed that the residence time in the bloodstream of 20kDa PVA-coated liposomes and 2kDa PEG were similar ²⁴. In the present study, PVA was characterized by a molecular weight ranging from 30 to 70 kDa while the one of PEG was about 5 kDa.



Figure 6: T_1 -weighted MRI of the liver in the coronal views after intravenous injection of NP3 in healthy rat before (A), 5 min (B) and 20 minutes (C) after intravenous injection.

The presence of gadolinium ions in the organic shell of AuNP confers to NP3 a behavior of positive contrast for MRI. The liver of a healthy rat was observed by MRI at different time points following the intravenous injection of NP3 (Figure 6). T_1 -weighted MR images in the coronal view showed a positive contrast enhancement in liver, 5 and 20 minutes after intravenous injection of NP3. This demonstrates a hepatic tropism of NP3 and confirms the preservation of imaging properties of gadolinium chelates-coated AuNP entrapped in the PLGA matrix.

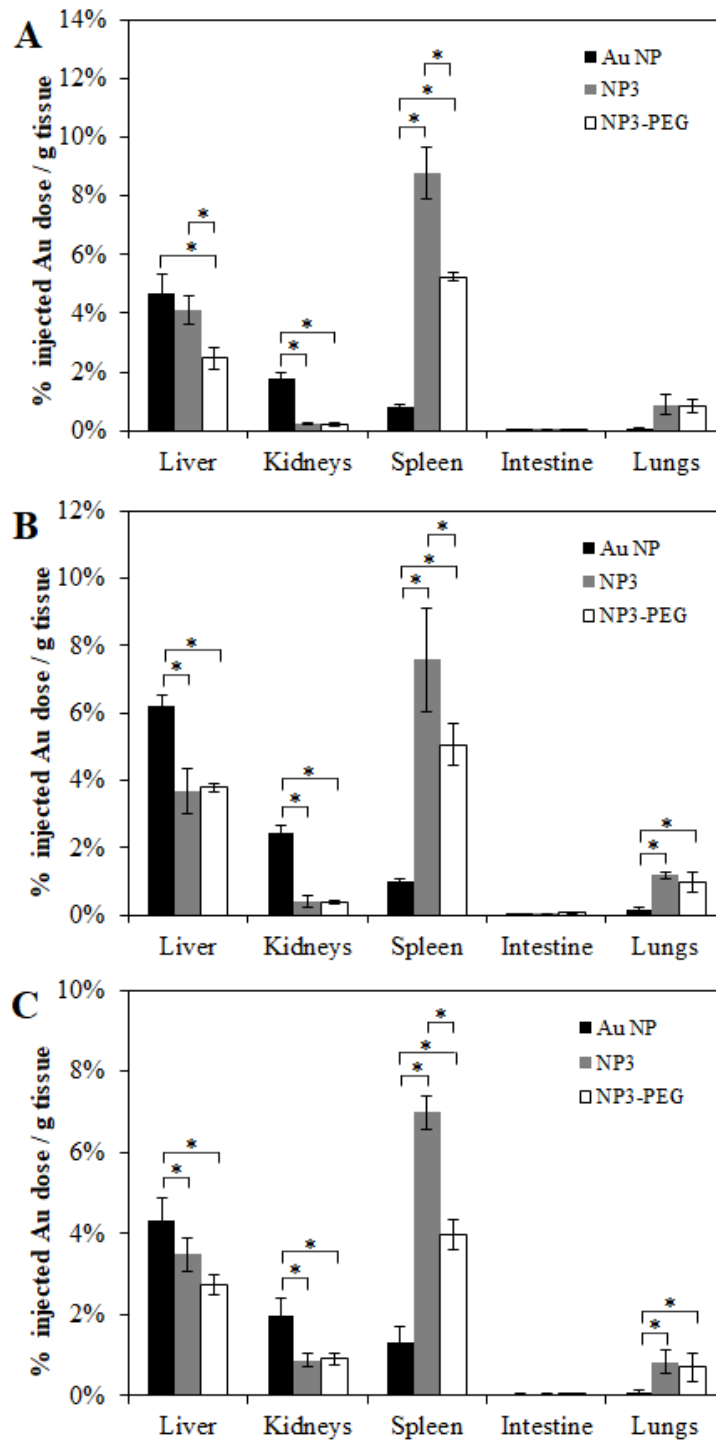


Figure 7: Biodistribution of AuNP, NP3 and NP3-PEG (PEI/Au=5) at 0.5h (A), 2 h (B) and 24h (C) following a single intravenous injection in healthy rat. Values were reported as mean \pm standard deviation (n=5 except for the NP3-PEG treatment where n=4). Statistical significance differences were determined according to an ANOVA test followed by a Turkey test except for lungs 0.5h where

variances were not equal (ANOVA on ranks). Results were considered as statistically significant at $P < 0.05$ (*).

For evaluating the effects of the encapsulation, the biodistribution of NP3 was compared to NP3-PEG and single AuNP. Organs were collected at 0.5h, 2h and 24h following the intravenous injection. Gold content was measured by ICP-AES (Figure 7). The AuNP were mainly detected in the liver and the kidneys and at a lower level, in the spleen. Surprisingly, the uptake of single AuNP per g tissue was higher in the liver than in the kidney despite their small size. At 0.5h, the percentage of injected doses per g tissue were of $4.7\% \pm 0.7\%$ and $1.8\% \pm 0.2\%$ in the liver and in the kidneys, respectively. Owing to their small size, AuNP could reach the space of Disse and interact with hepatocytes, inducing their degradation²⁵. Phagocytosis process was not considered due to the low gold content in macrophages-rich organs such as the spleen and the the lungs. Thus, a dual elimination mechanism of AuNP is suggested: renal excretion and hepatobiliary elimination. In figure 7, encapsulation of AuNP in NP3 and NP3-PEG changed their biodistribution. As expected, the accumulation of AuNP in kidneys was largely reduced after encapsulation. The preponderant uptake of both polymeric NP in liver, spleen and lungs demonstrates their recognition by the mononuclear phagocyte system, especially the Kuppfer cells, splenic and alveolar macrophages. However, the amount of NP3 and NP3-PEG in the liver stayed lower than small AuNP. This supports the hypothesis two hepatic elimination pathways of NP: the hepatobiliary route for AuNP able to reach the hepatocytes and the phagocytic route for large NP. The hepatic sequestration was significantly reduced with the PEG coating at 0.5h following the injection. The injected doses were of $4.1\% \pm 0.5\%$ and $2.5\% \pm 0.4\%$ for NP3 and NP3-PEG. The PLGA-PEG limited also the splenic sequestration compared with PLGA for the three time points. These results reveal a higher accumulation of NP3 in spleen and liver compared with NP3-PEG despite the steric barrier conferred by the PVA. Moghimi et al. showed hydrophilic coating with “brush-like” conformation reduces the phagocytosis of NP rather than a mushroom conformation²⁶. Adsorption of PVA on NP3 could induce the spreading of the stabilizer on the PLGA surface, justifying the mushroom conformation in contrast to PEG conjugated to PLGA. However, these differences between NP3 and NP3-PEG were not large enough to impact the vascular residence time of polymeric NP. Finally, the comparative

biodistribution study revealed major changes in the pharmacokinetic and distribution profiles of AuNP when encapsulated owing to both the increase in size and the difference in the chemical composition of the outer surface of AuNP, NP3 and NP3-PEG.

4. Conclusion

This work demonstrates the feasibility to efficiently load multifunctional AuNP in PLGA and PLGA-PEG nanocarriers using a polycation. Imaging properties of Gd anchored at the surface of AuNP was preserved as demonstrated by T_1 -weighted magnetic resonance imaging. The encapsulation improved both the uptake of AuNP in cancer cells through a passive mechanism and the vascular residence time for a better target tissue accumulation. The encapsulation of AuNP impacted their elimination pathway due to the large size of PLGA NP. Phagocytic route was demonstrated for large NP whereas both hepatobiliary mechanism and renal excretion were suggested for AuNP. A 24hr exposure of particles to a hepatocyte cell-line did not reveal any toxicity, demonstrating their safety. Thus, PLGA NP loaded with gadolinium chelates-coated AuNP exhibiting both contrast agent and radiosensitizing properties meet all the requirements for applications in imaging and radiotherapy of cancers. This technology paves the way to innovative imaging-guided anticancer therapies in personalized medicine.

Declaration of Competing Interest

The authors report no declarations of interest.




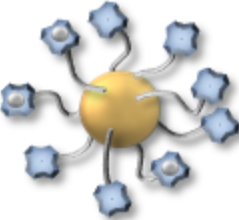
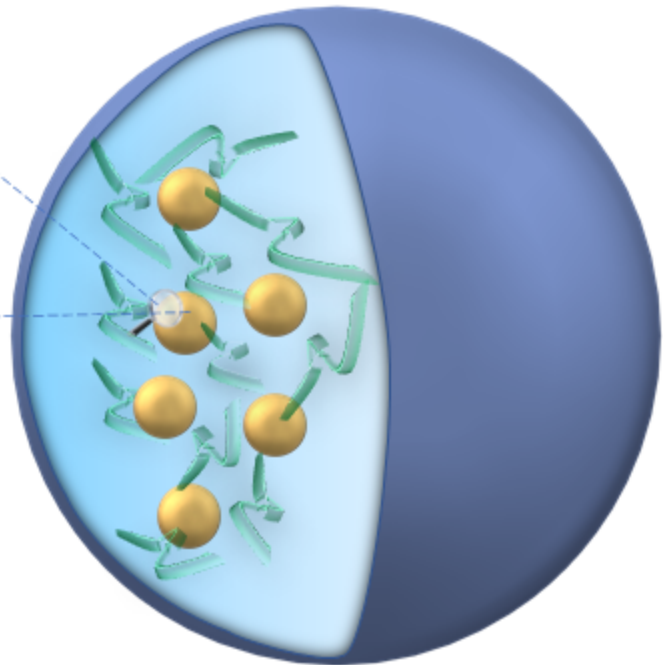
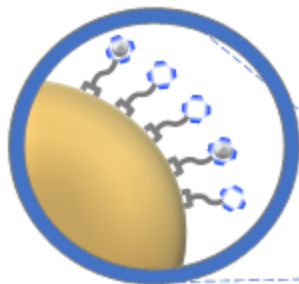

Acknowledgments

The authors thank Raphael Cornu for his help in the statistical analysis of results, Remi Chassagnon for the TEM acquisition and Qualio Laboratory (Besançon, France), especially Sylvaine Linget, for the gold analysis by ICP-OES. This project was funded by the French “Investissements d’Avenir” program, project ISITE-BFC (contract ANR-15-IDEX-0003, BIONANOCAR).

References

- 1 K. T. Butterworth, J. R. Nicol, M. Ghita, S. Rosa, P. Chaudhary, C. K. McGarry, H. O. McCarthy, G. Jimenez-Sanchez, R. Bazzi, S. Roux, O. Tillement, J. A. Coulter and K. M. Prise, *Nanomedicine (Lond)*, 2016, **11**, 2035–2047.
- 2 G. Laurent, C. Bernhard, S. Dufort, G. Jiménez Sánchez, R. Bazzi, F. Boschetti, M. Moreau, T. H. Vu, B. Collin, A. Oudot, N. Herath, H. Requardt, S. Laurent, L. Vander Elst, R. Muller, M. Dutreix, M. Meyer, F. Brunotte, P. Perriat, F. Lux, O. Tillement, G. Le Duc, F. Denat and S. Roux, *Nanoscale*, 2016, **8**, 12054–12065.
- 3 X. Yang, M. Yang, B. Pang, M. Vara and Y. Xia, *Chem. Rev.*, 2015, **115**, 10410–10488.
- 4 Y. Liu, P. Zhang, F. Li, X. Jin, J. Li, W. Chen and Q. Li, *Theranostics*, 2018, **8**, 1824–1849.
- 5 S. Rosa, C. Connolly, G. Schettino, K. T. Butterworth and K. M. Prise, *Cancer Nanotechnol*, 2017, **8**, 2.
- 6 K. Haume, S. Rosa, S. Grellet, M. A. Śmiałek, K. T. Butterworth, A. V. Solov'yov, K. M. Prise, J. Golding and N. J. Mason, *Cancer Nanotechnol*, 2016, **7**, 8.
- 7 J. Schuemann, R. Berbeco, D. B. Chithrani, S. H. Cho, R. Kumar, S. J. McMahon, S. Sridhar and S. Krishnan, *Int. J. Radiat. Oncol. Biol. Phys.*, 2016, **94**, 189–205.
- 8 H. Maeda, J. Fang, T. Inutsuka and Y. Kitamoto, *International Immunopharmacology*, 2003, **3**, 319–328.
- 9 K. T. Butterworth, S. J. McMahon, F. J. Currell and K. M. Prise, *Nanoscale*, 2012, **4**, 4830–4838.
- 10 H. S. Choi, W. Liu, P. Misra, E. Tanaka, J. P. Zimmer, B. Itty Ipe, M. G. Bawendi and J. V. Frangioni, *Nat. Biotechnol.*, 2007, **25**, 1165–1170.
- 11 M. Yu and J. Zheng, *ACS Nano*, 2015, **9**, 6655–6674.
- 12 J. S. Suk, Q. Xu, N. Kim, J. Hanes and L. M. Ensign, *Adv Drug Deliv Rev*, 2016, **99**, 28–51.
- 13 R. Gref, M. Lück, P. Quellec, M. Marchand, E. Dellacherie, S. Harnisch, T. Blunk and R. Müller, *Colloids Surf B Biointerfaces*, 2000, **18**, 301–313.
- 14 M. Brust, J. Fink, D. Bethell, D. J. Schiffrin and C. Kiely, *J. Chem. Soc., Chem. Commun.*, 1995, **0**, 1655–1656.
- 15 H. Fessi, F. Puisieux, J. P. Devissaguet, N. Ammoury and S. Benita, *International Journal of Pharmaceutics*, 1989, **55**, R1–R4.
- 16 H. Katas, E. Cevher, HO Alpar. *International Journal of Pharmaceutics*, 2009, 369(1-2), 144-54
- 17 M. Beck-Broichsitter, E. Rytting, T. Lehardt, X. Wang and T. Kissel, *Eur J Pharm Sci*, 2010, **41**, 244–253.
- 18 E. Luque-Michel, A. Larrea, C. Lahuerta, V. Sebastian, E. Imbuluzqueta, M. Arruebo, M. J. Blanco-Prieto and J. Santamaría, *Nanoscale*, 2016, **8**, 6495–6506
- 19 Y. Wang, E. M. Strohm, Y. Sun, Z. Wang, Y. Zheng, Z. Wang and M. C. Kolios, *Biomed Opt Express*, 2016, **7**, 4125–4138.

- 20 H. Kobayashi, S. Kawamoto, M. Bernardo, M. W. Brechbiel, M. V. Knopp and P. L. Choyke, *J Control Release*, 2006, **111**, 343–351.
- 21 S. Vranic, N. Boggetto, V. Contremoulins, S. Mornet, N. Reinhardt, F. Marano, A. Baeza-Squiban and S. Boland, *Part Fibre Toxicol*, 2013, **10**, 2.
- 22 B. D. Chithrani, A. A. Ghazani and W. C. W. Chan, *Nano Lett.*, 2006, **6**, 662–668.
- 23 B. D. Chithrani and W. C. W. Chan, *Nano Letters*, 2007, **7**, 1542–1550.
- 24 H. Takeuchi, H. Kojima, H. Yamamoto and Y. Kawashima, *J Control Release*, 2001, **75**, 83–91.
- 25 Y.-N. Zhang, W. Poon, A. J. Tavares, I. D. McGilvray and W. C. W. Chan, *Journal of Controlled Release*, , DOI:10.1016/j.jconrel.2016.01.020.
- 26 S.M. Moghimi, *FEBS Letters*, 2003, **540**, 241-244.

 : PVA : PEI : PLGA : Au@TADOTAGA : Gd³⁺